Nanoscale Advances

ROYAL SOCIETY OF CHEMISTRY

PAPER

View Article Online
View Journal | View Issue

Cite this: *Nanoscale Adv.*, 2023, **5**, 6249

A numerical study on the flow of water-based ternary hybrid nanomaterials on a stretchable curved sheet

W. Shinwari, *[a] T. Hayat,[a] Z. Abbas[b] and S. Momani[c]

Nanomaterials are quite promising in electronic cooling systems, heat exchangers, engine lubricants, brake liquids, shock absorbers, radiators, *etc.* Therefore, the study of heat transfer characteristics on the flow of trihybrid nanofluids on an exponentially stretched curved surface is developed. Purpose: In this study, trihybrid nanofluid is taken into consideration, which is composed of Fe_3O_4, Ag and Cu as nanoparticles and water as the basefluid. Heat generation and magnetic field impacts are addressed. Based on these assumptions, the governing partial differential equations were reduced to a favorable set of ordinary differential equations using adequate transformations. Formulation: The highly nonlinear coupled system of equations was numerically solved using the shooting method with the Runge–Kutta–Fehlberg technique. Findings: Trihybrid nanofluids improve the thermal performance of fluid when compared with other fluids such as hybrid nanofluids, nanofluids, and basefluids. The trihybrid nanofluid is efficient in heat transfer phenomenon and has a significant impact on the overall performance of a system, including cooling systems, heat exchangers, electronics, and many industrial processes. Graphical representation for the physical variables of the fluid velocity and temperature is discussed. The local Nusselt number and skin friction coefficient are computed and analyzed. A magnetic field decreases the velocity but escalates the temperature. The Nusselt number decreases for larger solid volume fractions. Novelty: The Tiwari and Das model for hybrid nanofluid extended for trihybrid nanoparticles has not been investigated previously. Heat transfer examination on the flow of trihybrid nanomaterials on exponentially curved stretching sheets considering magnetism force and heat generation consequence has not yet been studied.

Received 29th July 2023
Accepted 28th September 2023

DOI: 10.1039/d3na00572k

rsc.li/nanoscale-advances

1. Introduction

Heat transfer during flow is involved in numerous engineering applications such as glass fibre, plastic film drawing, chemical engineering plants, and copper wire annealing. The fundamental concept of heat transfer is based on the argument that heat is transmitted either to remove or to add energy to the system once it has been formed. In view of these investigations, the examination of the power law model for a laminar heat transfer flow was analyzed by Acrivos *et al.*[1] Steady flow with Newtonian heating was explored by Salleh *et al.*[2] Xu and Liao[3] studied heat transfer for the flow of non-Newtonian liquids. The impact on the MHD flow and heat transfer subject to the slip condition across a moving flat plate was deliberated by Ellahi *et al.*[4] They also examined the effects of entropy generations and numerically solved the boundary layer flow using the bvp4c Matlab technique. Khan *et al.*[5] mathematically formulated viscoelastic flow and heat transfer across an exponentially stretched surface. A mixed convection boundary layer flow caused by a stretching vertical sheet was examined by Ishak *et al.*[6] Bhattacharyya[7] worked on the heat transfer in a flow using an exponentially contracting sheet. Numerical studies on the transfer flow have been addressed by numerous researchers (see ref. 8–10).

Numerous industrial, technological, and manufacturing processes depend on the fluid flow involving the curved stretched sheets. A few applications include paper production, hot rolling, polymer extrusion, and glass-fiber production. Sajid *et al.*[11] reported viscous fluid flow resulting from a curved stretching sheet. They found similar solutions for the boundary value problem using the Runge–Kutta approach. Numerous features of flow and

[a]*Department of Mathematics, Quaid-I-Azam University, Islamabad 44000, Pakistan. E-mail: wajeeha.shinwari2014@gmail.com*

[b]*Department of Mathematics, The Islamia University of Bahawalpur, Bahawalpur 63100, Pakistan*

[c]*Nonlinear Dynamics Research Center (NDRC), Ajman University, Ajman, United Arab Emirates*

W. Shinwari is PhD scholar at Department of Mathematics, Quaid-I-Azam University 45320, Islamabad 44000, Pakistan.

T. Hayat is Professor at Department of Mathematics, Quaid-I-Azam University 45320, Islamabad 44000, Pakistan.

heat transmission processes by curved stretchable sheets have been examined by Naveed *et al.*[12] Ahmed *et al.*[13] addressed a numerical study of a mixed convective flow over an exponentially stretched curved sheet. An overview of the hydromagnetic flow on a curved stretched sheet with heat transfer was reported by Abbas *et al.*[14] A second-grade fluid flow with Stefan blowing effect for curved stretched sheets was studied by Punith Gowda[15] Khan *et al.*[16] published a theoretical analysis on heat transfer in CNTs-water nanofluid on curved surfaces. Flow induced by a curved sheet with a heated, exponentially stretching velocity was addressed by Wahid and colleagues.[17] Radiative CNT-based hybrid MHD flow over a curved surface with slippage and convective heating was explored by Ali *et al.*[18]

Basically, a nanofluid (NF) is a suspension of solid nanosized particles (1–100 nm) in traditional baseliquids. Applications of nanoparticles are found in various engineering and industrial processes, such as electronics cooling facilities, heat exchangers, solar collectors, and air conditioning process. These materials are employed to enhance the heat transfer and thermal decomposition capabilities. Nanoparticles may exist in different forms such as carbides, carbon nanotubes, metal oxides, and metals nitrides. The basefluids may include engine oil, ethylene glycol, kerosene oil, and water. Problems of the MHD nanofluid with radiation and heat source/sink effects were previously investigated by Mohana and Kumar.[19] Numerical investigations on magnetic nanofluids with thermal radiation effects using a stretching sheet were carried out by Kumar and Kumar.[20] Another new category of nanofluids with advanced thermophysical properties is called hybrid nanomaterials. These comprise different nanoparticles suspended in a liquid base. In order to increase the thermal conductivity in various heat transport systems, such as automobile radiators, generator cooling, engines, building heating, and biomedicine, hybrid nanofluids have been introduced. Furthermore Ullah[21] constructed a numerical investigation of the MHD flow of hybrid nanofluids. Ahmed *et al.*[22] examined nonlinear radiation and chemical reaction effects for the (Cu–CuO)/NaAlg hybrid nanofluid by a stretchable surface. Lu *et al.*[23] considered hybrid nanoliquid coatings with nonlinear radiation and entropy generation in the flow on a curved stretching sheet. Model-based comparison of unstable hybrid nanofluid flow with particle shape effects in magnetohydrodynamics has been reported by Chu *et al.*[24] Sadiq *et al.*[25] examined hybrid nanomaterials with variable properties for the Darcy–Forchheimer–Brinkman porous space. Jana *et al.*[26] performed an analysis on thermal conductivity enhancement through hybrid NF. Numerical analysis of 3D MHD hybrid nanomaterials was performed by Devi and Devi.[27] Nadeem *et al.*[28] studied the flow of hybrid nanoparticles on a permeable nonlinear stretching curved sheet. Nabwey and Mahdy[29] examined the transient MHD flow for hybrid nanomaterial (Fe_3O_4–Ag). The chemical reaction and heat generation of a Ag–CuO/ water hybrid nanofluid over a stretchable surface with rotation was investigated by Hayat and Nadeem.[30] Increased thermal potential of Maxwell hybrid NF due to the stretched sheet in addition to kerosene oil, silver, and graphene oxide was studied by Ahmad *et al.*[31] Trihybrid nanofluids are considered an expansion of a hybrid nanofluids, which may include three distinct nanoparticles in typical liquids either in combined or dispersed forms. Haneef *et al.*[32] highlighted the model (THNF) for the Maxwell fluid and initiated the solution of heat and mass transfer for trihybrid Al_2O_3, TiO_2 and SiO_2, and monohybrid nanomaterials. With the help of nanoparticles TiO_2, Al_2O_3 and SiO_2 suspended in water, the ternary NF were studied for heat transfer flow using a stretched sheet in Manjunatha *et al.*[33] The stability analysis of trihybrid nanofluids distributed through a water-ethylene glycol mixture was reported in one attempt.[34] Hasnain and Abid[35] investigated the flow problem of heat transfer in 3D ternary hybrid NF using water and motor oil as base fluids in both nonlinear and linear stretching sheets. Sohail and Zahar[36] demonstrated thermal increases for trihybrid nanomaterials in a mixture of pseudo-plastic fluid using the FEM method. Various attempts on trihybrid nanofluids have been attempted in previous studies.[37–42] Furthermore, Sparrow *et al.*[43] employed a technique for solving the non-similar problems. Raees *et al.*[44] inspected the results for the mixed convection flow of the magnetized second-grade nanofluid in this direction. Patil *et al.*[45] developed solutions for 2D double-diffusive mixed convection flows across a porous exponentially stretching sheet. The Darcy–Forchheimer–Brinkman model was used to examine Casson fluid flow by Farooq *et al.*[46] Ray *et al.*[47] proposed a solution for the mixed convection flow of an Eyring–Powell material. Homotopy analysis was employed.

Trihybrids nanofluids have wide applications in industrial and engineering fields, including the cooling system, heat exchangers, automobile radiators, and biomedicine. The aim of this study was to investigate the effects of a water-based trihybrid nanofluid on an exponentially curved stretching sheet. Additionally, our work is an expansion of many previous studies. The Tiwari and Das model for hybrid nanofluid is further expanded for trihybrid nanofluid to obtain a better heat conductor than hybrid nanofluid. This is a new study after the inclusion of MHD and heat generation.

This communication addresses the following objectives and points.

(1) Comparative study of the MHD flow of trihybrid nanoparticles (Fe_3O_4, Ag, and Cu) in water as a base fluid.

(2) Trihybrid nanofluid (thnf) is modeled for flow on a curved stretched surface.

(3) A numerical approach named the RK Fehlberg method was employed for local similar solution development.

(4) The flow by an exponentially stretched sheet was examined.

(5) The local Nusselt number and skin friction coefficient were examined in addition to velocity and temperature.

(6) Streamline analysis was sketched for various parameters.

Z. Abbas is Professor at Department of Mathematics, The Islamia University of Bahawalpur, Bahawalpur 63100, Pakistan.

S. Momani is Professor at Nonlinear Dynamics Research Center (NDRC), Ajman University, Ajman, United Arab Emirates.

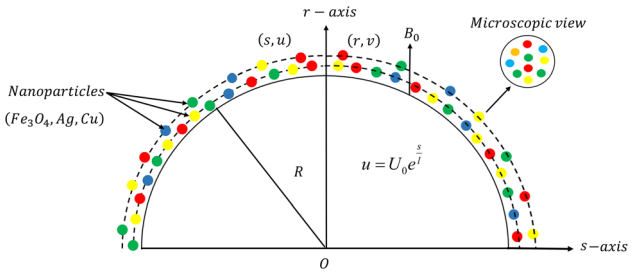

Fig. 1 Flow diagram.[48]

2. Mathematical formulation

A two-dimensional steady flow of trihybrid nanomaterials on a curved stretching surface was considered. The curved surface with a radius of curvature R was stretched. Here s was directed along the flow and r at any point on the surface normal to the tangent (see Fig. 1). Stretching velocity being $u = U_0 e^{\frac{s}{l}}$, in which U_0 acts as a reference velocity. A magnetic field of constant strength B_0 along r was exerted. The magnetic Reynolds number is low and the consequently induced magnetic field was negligible. Heat generation and ohmic heating were observed. The following fundamental equations of trihybrid NF are provided using previous assumptions and boundary layer approximations:[11–18]

$$\frac{\partial}{\partial r}((r+R)v) + R\frac{\partial u}{\partial s} = 0, \tag{1}$$

$$\frac{u^2}{r+R} = \frac{1}{\rho_{\text{thnf}}}\frac{\partial p}{\partial r}, \tag{2}$$

$$\left.\begin{aligned} v\frac{\partial u}{\partial r} + \frac{uR}{r+R}\frac{\partial u}{\partial s} + \frac{uv}{r+R} &= -\frac{1}{\rho_{\text{thnf}}}\frac{R}{r+R}\frac{\partial p}{\partial s} \\ &+ \frac{\mu_{\text{thnf}}}{\rho_{\text{thnf}}}\left(\frac{\partial^2 u}{\partial r^2} + \frac{1}{r+R}\frac{\partial u}{\partial r} - \frac{u}{(r+R)^2}\right) - \frac{\sigma_{\text{thnf}}}{\rho_{\text{thnf}}}B_0^2 u \end{aligned}\right\}, \tag{3}$$

$$v\frac{\partial T}{\partial r} + \frac{uR}{r+R}\frac{\partial T}{\partial s} = \frac{k_{\text{thnf}}}{(\rho c_{\text{p}})_{\text{thnf}}}\left(\frac{\partial^2 T}{\partial r^2} + \frac{1}{r+R}\frac{\partial T}{\partial r}\right) + \frac{\sigma_{\text{thnf}}}{(\rho c_{\text{p}})_{\text{thnf}}}B_0^2 u^2 + \frac{Q_0}{(\rho c_{\text{p}})_{\text{thnf}}}(T - T_\infty). \tag{4}$$

In the above expressions u and v stand for velocity components in $s-$ and $r-$ directions, respectively, and Q_0 (>0), the heat generation coefficient. Additionally $(\rho c_{\text{p}})_{\text{thnf}}$, σ_{thnf}, μ_{thnf}, k_{thnf} and ρ_{thnf} are heat capacity, electric conductivity, dynamic viscosity, thermal conductivity, and density of trihybrid nanomaterials, respectively.

The conditions for this problem are expressed as

$$u = u_{\text{w}} = U_0 e^{\frac{s}{l}}, \quad v = 0, \quad T = T_{\text{w}}\left(T_{\text{w}} = T_\infty + T_0 e^{\frac{A_0 s}{2l}}\right) \tag{5}$$

at $r = 0$,

$$u \to 0, \quad \frac{\partial u}{\partial r} \to 0, \quad T \to T_\infty \quad \text{as } r \to \infty, \tag{6}$$

where T indicates the fluid temperature, A_0 is the temperature exponent, T_0 is the reference temperature, and T_∞ is the ambient temperature (Tables 1–3).Here ϕ_i, k_i, ρ_i and σ_i $(i = 1$ to 3) indicate the solid volume fractions, thermal conductivities, density and electric conductivities of Fe_3O_4, Ag and Cu, respectively.

Table 1 Novelty of the present study

Ref. no	5	13	32	48	52	Present
Exponentially stretching curved sheet	No	Yes	No	No	Yes	Yes
Trihybrid fluid	No	No	Yes	Yes	No	Yes
Numerical solution	Yes	Yes	Yes	Yes	Yes	Yes
Magnetic field	No	Yes	Yes	No	No	Yes
Heat generation	No	No	Yes	Yes	Yes	Yes

Table 2 Physical properties of thermodynamics for trihybrid nanoparticles (thnf)[49]

Properties	Correlations
Density	$\rho_{\text{thnf}} = (1-\phi_1)\{(1-\phi_2)[(1-\phi_3)\rho_{\text{f}} + \phi_3\rho_3] + \phi_2\rho_2\} + \phi_1\rho_1$
Viscosity	$\mu_{\text{thnf}} = \frac{\mu_{\text{f}}}{(1-\phi_1)^{2.5}(1-\phi_2)^{2.5}(1-\phi_3)^{2.5}}$
Thermal conductivity	$\frac{k_{\text{thnf}}}{k_{\text{hnf}}} = \frac{k_1 + 2k_{\text{hnf}} - 2\phi_1(k_{\text{hnf}} - k_1)}{k_1 + 2k_{\text{hnf}} + \phi_1(k_{\text{hnf}} - k_1)}$, $\frac{k_{\text{hnf}}}{k_{\text{nf}}} = \frac{k_2 + 2k_{\text{hnf}} - 2\phi_2(k_{\text{nf}} - k_2)}{k_2 + 2k_{\text{hnf}} + \phi_2(k_{\text{nf}} - k_2)}$ $\frac{k_{\text{nf}}}{k_{\text{f}}} = \frac{k_3 + 2k_{\text{f}} - 2\phi_3(k_{\text{f}} - k_3)}{k_3 + 2k_{\text{f}} + \phi_3(k_{\text{f}} - k_3)}$
Electric conductivity	$\frac{\sigma_{\text{thnf}}}{\sigma_{\text{hnf}}} = \frac{\sigma_1 + 2\sigma_{\text{hnf}} - 2\phi_1(\sigma_{\text{hnf}} - \sigma_1)}{\sigma_1 + 2\sigma_{\text{hnf}} + \phi_1(\sigma_{\text{hnf}} - \sigma_1)}$, $\frac{\sigma_{\text{hnf}}}{\sigma_{\text{nf}}} = \frac{\sigma_2 + 2\sigma_{\text{nf}} - 2\phi_2(\sigma_{\text{nf}} - \sigma_2)}{\sigma_2 + 2\sigma_{\text{nf}} + \phi_2(\sigma_{\text{nf}} - \sigma_2)}$ $\frac{\sigma_{\text{nf}}}{\sigma_{\text{f}}} = \frac{\sigma_3 + 2\sigma_{\text{f}} - 2\phi_3(\sigma_{\text{f}} - \sigma_3)}{\sigma_3 + 2\sigma_{\text{f}} + \phi_3(\sigma_{\text{f}} - \sigma_3)}$
Heat capacity	$(\rho c_{\text{p}})_{\text{thnf}} = \phi_1(\rho c_{\text{p}})_1 + \phi_2(\rho c_{\text{p}})_2 + \phi_3(\rho c_{\text{p}})_3 + (1-\phi_1-\phi_2-\phi_3)(\rho c_{\text{p}})_{\text{f}}$

Table 3 Thermophysical values of baseliquid and nanoparticles[50–52]

	Base fluid	Nanoparticles		
Physical properties	H_2O	Fe_3O_4 (ϕ_1)	Ag (ϕ_2)	Cu (ϕ_3)
ρ (Kg m^{-3})	997.1	5180	10 500	8933
k (W mK^{-1})	0.613	9.7	429	401
C_p (J kg^{-1} K^{-1})	4179	670	235	385

$$\frac{\partial f}{\partial \eta}(\xi,\infty)\to 0,\quad \frac{\partial^2 f}{\partial \eta^2}(\xi,\infty)\to 0,\quad \theta(\xi,\infty)\to 0 \quad \text{as } \eta\to\infty, \tag{12}$$

where $(\rho c_p)_f$, σ_f, ρ_f and k_f are heat capacity, electric conductivity, density, and thermal conductivity of the base fluid, respectively, K is the curvature parameter, λ (>0) is the heat generation parameter, Ec is the Eckert number, Pr is the Prandtl number, and M is the magnetic parameter. These variables are defined as

Considering the transformations[53]

$$\left.\begin{aligned} u &= U_0 e^{\frac{s}{l}}\frac{\partial f(\xi,\eta)}{\partial \eta},\quad v = -\frac{R}{r+R}\sqrt{\frac{v_f U_0 e^{\frac{s}{l}}}{2l}}\left(f(\xi,\eta)+2\xi\frac{\partial f(\xi,\eta)}{\partial \xi}+\eta\frac{\partial f(\xi,\eta)}{\partial \eta}\right)\\ p &= \rho_f U_0^2 e^{\frac{2s}{l}}P(\xi,\eta),\quad \theta(\xi,\eta)=\frac{T-T_\infty}{T_0 e^{\frac{A_0 s}{2l}}},\quad T = T_\infty + T_0 e^{\frac{A_0 s}{2l}}\theta(\xi,\eta)\\ \eta &= \sqrt{\frac{U_0 e^{\frac{s}{l}}}{2v_f l}}r,\quad \xi = e^{\frac{s}{l}} \end{aligned}\right\}, \tag{7}$$

Eqn (1) is satisfied trivially and eqn (2)–(6) become

$$\frac{\partial P}{\partial \eta} = \frac{\rho_{thnf}}{\rho_f}\frac{1}{(\eta+K\sqrt{\xi})}\left(\frac{\partial f}{\partial \eta}\right)^2, \tag{8}$$

$$\left.\begin{aligned} &\frac{\rho_f}{\rho_{thnf}}\frac{4K\sqrt{\xi}}{(\eta+K\sqrt{\xi})}P+\frac{\rho_f}{\rho_{thnf}}\frac{2K}{(\eta+K\sqrt{\xi})}\xi^{\frac{3}{2}}\frac{\partial P}{\partial \xi}+\frac{\rho_f}{\rho_{thnf}}\frac{K\sqrt{\xi}}{(\eta+K\sqrt{\xi})}\eta\frac{\partial P}{\partial \eta} = \frac{K\sqrt{\xi}}{(\eta+K\sqrt{\xi})}f\frac{\partial^2 f}{\partial \eta^2}\\ &+\frac{2K}{(\eta+K\sqrt{\xi})}\xi^{\frac{3}{2}}\frac{\partial f}{\partial \xi}\frac{\partial^2 f}{\partial \eta^2}-\frac{2K\sqrt{\xi}}{(\eta+K\sqrt{\xi})}\left(\frac{\partial f}{\partial \eta}\right)^2-\frac{2K}{(\eta+K\sqrt{\xi})}\xi^{\frac{3}{2}}\frac{\partial^2 f}{\partial \xi\partial \eta}\frac{\partial f}{\partial \eta}\\ &+\frac{K\sqrt{\xi}}{(\eta+K\sqrt{\xi})^2}f\frac{\partial f}{\partial \eta}+\frac{2K}{(\eta+K\sqrt{\xi})^2}\xi^{\frac{3}{2}}\frac{\partial f}{\partial \xi}\frac{\partial f}{\partial \eta}+\frac{K\sqrt{\xi}}{(\eta+K\sqrt{\xi})^2}\eta\left(\frac{\partial f}{\partial \eta}\right)^2\\ &+\frac{\nu_{nf}}{\nu_f}\left[\frac{\partial^3 f}{\partial \eta^3}+\frac{1}{(\eta+K\sqrt{\xi})}\frac{\partial^2 f}{\partial \eta^2}-\frac{1}{(\eta+K\sqrt{\xi})^2}\frac{\partial f}{\partial \eta}\right]-\frac{\sigma_{thnf}}{\sigma_f}\frac{\rho_f}{\rho_{thnf}}\frac{2M}{\xi}\frac{\partial f}{\partial \eta} \end{aligned}\right\}, \tag{9}$$

$$\left.\begin{aligned} &\frac{k_{thnf}}{k_f}\left(\frac{\partial^2\theta}{\partial \eta^2}+\frac{1}{(\eta+K\sqrt{\xi})}\frac{\partial \theta}{\partial \eta}\right)+2\frac{(\rho c_p)_f}{(\rho c_p)_{thnf}}\frac{1}{\xi}\mathrm{Pr}\lambda\theta+2\frac{\sigma_{thnf}}{\sigma_f}\mathrm{PrEc}M\xi^{1-\frac{A_0}{2}}\left(\frac{\partial f}{\partial \eta}\right)^2\\ &=-\frac{(\rho c_p)_{thnf}}{(\rho c_p)_f}\mathrm{Pr}\frac{K\sqrt{\xi}}{(\eta+K\sqrt{\xi})}f\frac{\partial \theta}{\partial \eta}+\frac{(\rho c_p)_{thnf}}{(\rho c_p)_f}A_0\mathrm{Pr}\frac{K\sqrt{\xi}}{(\eta+K\sqrt{\xi})}\frac{\partial f}{\partial \eta}\theta\\ &-\frac{(\rho c_p)_{thnf}}{(\rho c_p)_f}\frac{2K}{(\eta+K\sqrt{\xi})}\xi^{\frac{3}{2}}\frac{\partial f}{\partial \xi}\frac{\partial \theta}{\partial \eta}+\frac{(\rho c_p)_{thnf}}{(\rho c_p)_f}\frac{2K}{(\eta+K\sqrt{\xi})}\xi^{\frac{3}{2}}\frac{\partial \theta}{\partial \xi}\frac{\partial f}{\partial \eta}, \end{aligned}\right\}, \tag{10}$$

with boundary conditions

$$f(\xi,0) = -2\xi\frac{\partial f}{\partial \xi}(\xi,0),\quad \frac{\partial f}{\partial \eta}(\xi,0)=1,\quad \theta(\xi,0)=1 \quad \text{at } \eta=0, \tag{11}$$

$$\left.\begin{aligned} K &= \sqrt{\frac{U_0}{2\nu_f l}}R, \quad \lambda = \frac{Q_0 l}{U_0(\rho c_p)_f} \quad \mathrm{Ec} = \frac{U_0^2}{T_0(c_p)_f} \\ \mathrm{Pr} &= \frac{\nu_f(\rho c_p)_f}{k_f}, \quad M = \frac{\sigma_f B_0^2 l}{\rho_f U_0} \end{aligned}\right\}. \tag{13}$$

To obtain local similar solutions the terms including the derivative with respect to $\xi\left(i.e.\frac{\partial(\cdot)}{\partial\xi}=0\right)$ are treated as zero in eqn (8)–(12). The resulting equations become

$$P' = \frac{\rho_{thnf}}{\rho_f}\frac{1}{(\eta+K\sqrt{\xi})}f'^2, \tag{14}$$

$$\left.\begin{aligned} &\frac{\rho_f}{\rho_{thnf}}\frac{4K\sqrt{\xi}}{(\eta+K\sqrt{\xi})}P + \frac{\rho_f}{\rho_{thnf}}\frac{K\sqrt{\xi}}{(\eta+K\sqrt{\xi})}\eta P' = \frac{K\sqrt{\xi}}{(\eta+K\sqrt{\xi})}ff'' - \frac{2K\sqrt{\xi}}{(\eta+K\sqrt{\xi})}(f')^2 + \frac{K\sqrt{\xi}}{(\eta+K\sqrt{\xi})^2}ff' \\ &+\frac{K\sqrt{\xi}}{(\eta+K\sqrt{\xi})^2}\eta(f')^2 + \frac{\nu_{nf}}{\nu_f}\left[f''' + \frac{1}{(\eta+K\sqrt{\xi})}f'' - \frac{1}{(\eta+K\sqrt{\xi})^2}f'\right] - \frac{\sigma_{thnf}}{\sigma_f}.\frac{\rho_f}{\rho_{thnf}}\frac{2M}{\xi}f' \end{aligned}\right\}, \tag{15}$$

$$\left.\begin{aligned} &\frac{k_{thnf}}{k_f}\left(\theta' + \frac{1}{(\eta+K\sqrt{\xi})}\theta'\right) + \frac{(\rho c_p)_{thnf}}{(\rho c_p)_f}\mathrm{Pr}\frac{K\sqrt{\xi}}{(\eta+K\sqrt{\xi})}f\theta' - \frac{(\rho c_p)_{thnf}}{(\rho c_p)_f}A_0\mathrm{Pr}\frac{K\sqrt{\xi}}{(\eta+K\sqrt{\xi})}f'\theta + 2\frac{\sigma_{thnf}}{\sigma_f}\mathrm{PrEc}M\xi^{1-\frac{A_0}{2}}(f')^2 \\ &+2\frac{(\rho c_p)_f}{(\rho c_p)_{thnf}}\mathrm{Pr}\lambda\frac{1}{\xi}\theta = 0 \end{aligned}\right\}, \tag{16}$$

with

$$\begin{aligned} &f(0)=0, \quad f'(0)=1, \quad \theta(0)=1 \quad \text{at } \eta=0, \\ &f'(\infty)=0, \quad f''(\infty)=0, \quad \theta(\infty)=0 \quad \text{as } \eta\to\infty. \end{aligned} \tag{17}$$

Neglecting the pressure terms from eqn (14) to (15) we obtain

$$\left.\begin{aligned} f^{iv} &= \frac{1}{A_1}\frac{K\sqrt{\xi}}{(\eta+K\sqrt{\xi})}(3f'f''-ff''') + \frac{1}{A_1}\frac{K\sqrt{\xi}}{(\eta+K\sqrt{\xi})^2}\left(3f'^2-ff''\right) + \frac{1}{A_1}\frac{K\sqrt{\xi}}{(\eta+K\sqrt{\xi})^3}ff' \\ &-\frac{2}{(\eta+K\sqrt{\xi})}f''' + \frac{1}{(\eta+K\sqrt{\xi})^2}f'' - \frac{1}{(\eta+K\sqrt{\xi})^3}f' + \frac{2M}{\xi}\frac{A_3}{A_1A_2}\left(f'' + \frac{1}{(\eta+K\sqrt{\xi})}f'\right) \end{aligned}\right\}, \tag{18}$$

where (A_1–A_5) are

$$\begin{aligned} &A_1 = \frac{\nu_{thnf}}{\nu_f}, \quad A_2 = \frac{\rho_{thnf}}{\rho_f}, \quad A_3 = \frac{\sigma_{thnf}}{\sigma_f}, \quad A_4 = \frac{k_{thnf}}{k_f}, \\ &A_5 = \frac{(\rho c_p)_{thnf}}{(\rho c_p)_f}. \end{aligned} \tag{19}$$

Using the above equation eqn (16) we obtain

$$\left.\begin{aligned} &\left(\theta'' + \frac{1}{(\eta+K\sqrt{\xi})}\theta'\right) + \frac{A_5}{A_4}\mathrm{Pr}\frac{K\sqrt{\xi}}{(\eta+K\sqrt{\xi})}f\theta' - \frac{A_5}{A_4}\mathrm{Pr}A_0\frac{K\sqrt{\xi}}{(\eta+K\sqrt{\xi})}f'\theta \\ &+2\frac{A_3}{A_4}\mathrm{PrEc}M\xi^{1-\frac{A_0}{A_2}}(f')^2 + 2\mathrm{Pr}\frac{1}{A_4}\frac{\lambda}{\xi}\theta = 0 \end{aligned}\right\}. \tag{20}$$

The Nusselt number and the coefficient of skin friction are[54]

$$N_{u_s} = \frac{sq_w}{k_f(T_w - T_\infty)}, \quad C_f = \frac{\tau_{rs}}{\rho_{thnf}u_w^2}, \tag{21}$$

in which q_w represents heat flux and τ_{rs} the wall shear stress, *i.e.*[54]

$$q_w = -k_{thnf}\left(\frac{\partial T}{\partial r}\right)_{r=0}, \quad \tau_{rs} = \mu_f\left(\frac{\partial u}{\partial r} - \frac{u}{(r+R)}\right)_{r=0}. \tag{22}$$

One can finally write as

$$N_{u_s}(\mathrm{Re}_s)^{-1/2} = -\frac{k_{thnf}}{k_f}\xi^{\frac{1}{2}}\ln(\xi)\theta'(0), \tag{23}$$

$$C_f(\mathrm{Re}_s)^{1/2} = \frac{\mu_{thnf}}{\mu_f}\frac{\xi^{-\frac{1}{2}}}{2}\left(f''(0) - \frac{1}{K\sqrt{\xi}}\right), \quad (24)$$

in which, $\mathrm{Re}_s = \frac{U_0 l}{2\nu_f}$ depicts the local Reynolds number.

3. Numerical procedure

Here, the shooting method in conjunction with the RK Fehlberg technique *via* MATLAB software was used. The shooting method transforms a boundary value problem into an initial value problem by guessing one of the boundary conditions using a numerical ordinary differential equations (ODEs) solver such as the RK Fehlberg method. The RK Fehlberg method, often referred to as the RK45 method, is a variant of the RK numerical integration technique. This is a method specifically designed to solve ODEs while adjusting the step size. This method has many advantages for solving initial value problems (IVPs) when both accuracy and efficiency are important. It also does not require manual adjustment of the parameters and provides adaptive step size control, which improves efficiency. The method is employed to solve dimensionless equations, *i.e.*, eqn (18) and (20), while taking into account the boundary conditions given in eqn (17). Firstly, we convert the boundary value system into a first-order ODE system by assuming.

$$\left.\begin{array}{llll} y(1) = f(\eta), & y(2) = f'(\eta), & y(3) = f''(\eta), & y(4) = f'''(\eta) \\ y(5) = \theta(\eta), & y(6) = \theta'(\eta) & & \end{array}\right\}, \quad (25)$$

We obtain

$$\begin{bmatrix} y'(1) \\ y'(2) \\ y'(3) \\ y'(4) \\ y'(5) \\ y'(6) \end{bmatrix} = \begin{bmatrix} y(2) \\ y(3) \\ y(4) \\ \frac{1}{A_1}\frac{K\sqrt{\xi}}{(\eta+K\sqrt{\xi})}\left\{\begin{array}{l}(3y(2)y(3) - y(1)y(4)) + \frac{1}{(\eta+K\sqrt{\xi})}(3y(2)y(2) - y(1)y(3)) \\ +\frac{1}{(\eta+K\sqrt{\xi})^2}y(1)y(2)\end{array}\right\} \\ -2\frac{1}{(\eta+K\sqrt{\xi})}y(4) + \frac{1}{(\eta+K\sqrt{\xi})^2}y(3) - \frac{1}{(\eta+K\sqrt{\xi})^3}y(2) + 2\frac{M}{\xi}\frac{A_3}{A_1A_2}\left(y(3) + \frac{y(2)}{(\eta+K\sqrt{\xi})}\right)y(6) \\ -\frac{1}{(\eta+K\sqrt{\xi})}y(6) - \frac{2}{A_4\xi}\mathrm{Pr}\lambda y(5) - \frac{A_5}{A_4}\frac{K\sqrt{\xi}}{(\eta+K\sqrt{\xi})}\mathrm{Pr}y(1)y(6) \\ +\frac{A_5}{A_4}\frac{K\sqrt{\xi}}{(\eta+K\sqrt{\xi})}A_0\mathrm{Pr}y(2)y(5) - 2\frac{A_3}{A_4}\mathrm{PrEc}M\xi^{\left(1-\frac{A_0}{2}\right)}y(2)y(2). \end{bmatrix}, \quad (26)$$

For the above system the initial conditions are as follows:

$$\begin{bmatrix} y(1) \\ y(2) \\ y(3) \\ y(4) \\ y(5) \\ y(6) \end{bmatrix} = \begin{bmatrix} 0 \\ 1 \\ u(1) \\ u(2) \\ 1 \\ u(3) \end{bmatrix}. \quad (27)$$

Here appropriate values are assumed for the initial conditions.

$$u(1) = f'',\ u(2) = f''',\ u(3) = \theta' \quad (28)$$

These are unknowns followed by the RK Fehlberg technique.

4. Analysis

Analysis of Fe_3O_4, Ag and Cu nanoparticles with water as a base fluid under the behavior of emerging parameters including magnetic parameter M, curvature parameter K, Eckert number Ec, heat generation parameter λ, temperature exponent A_0, Prandtl number Pr and ξ are shown graphically in Fig. 2–12. The mathematical system of the equations was computed numerically. The stretching sheet behavior was observed using graphs. Furthermore, Fig. 13 and 14 show how the rate of heat transfer and surface drag force vary for the pertinent parameters. Table 4 indicates the validity and accuracy of the numerical results of the heat transfer coefficient for various values of Pr. The results were compared with those of Bidin and Nazar[55] and Khan *et al.*[53] and were found to be in good agreement. Clearly, it is observed

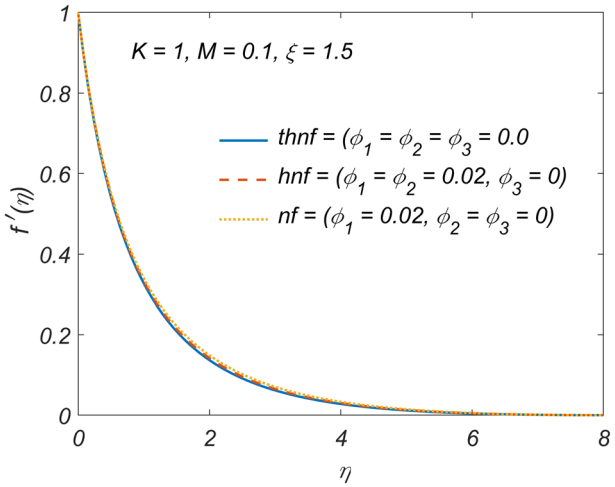

Fig. 2 Comparison of the three different fluids for velocity.

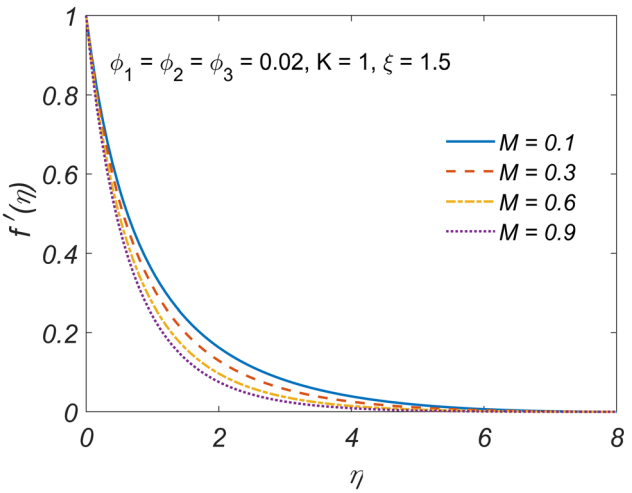

Fig. 3 Magnetic parameter against velocity.

that as Pr increases, the values of the heat transfer coefficient also increases.

4.1. Velocity

Fig. 2 depicts the comparison of trihybrid nanofluid, hybrid nanofluid, and nanofluid for the velocity field. Here, dotted lines show how the behavior of the stretching sheet is affected by nanoparticles, dashed lines correspond to hybrid nanoparticles, and the solid lines are related to the trihybrid nanoparticles. Here, the velocity of the trihybrid nanofluid is lower than that of other materials containing nanoparticles. Fig. 3 shows that the velocity and related layer thickness decrease upon improvement M. Clearly, an increase in the magnetic field acts as a resistance to fluid velocity and is associated with the production of Lorentz forces, which results in the decline of fluid velocity. As shown in Fig. 4, the flow velocity for all the types of nanofluids was noticeably increased as the curvature parameter for the curved stretching surface increases.

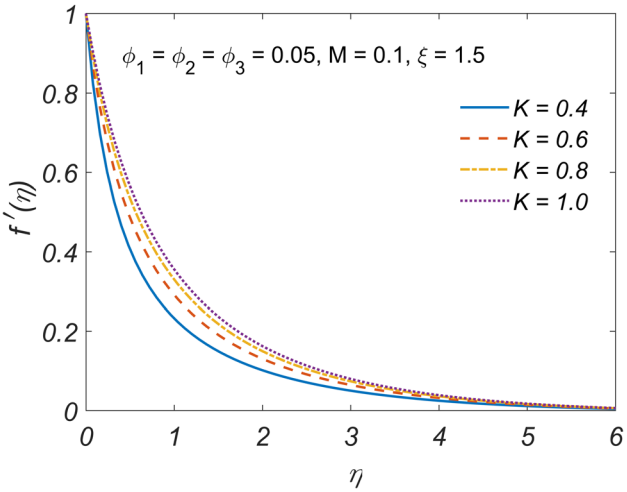

Fig. 4 Curvature parameter against velocity.

Physically, the curvature parameter is inversely proportional to the kinematic viscosity of the basefluid. Hence, for the higher estimation of the curvature parameter, the radius of the sheet also increases due to which fewer particles stick to the surface. Hence, low resistance leads to higher velocity. For the curved surface, the velocity is the highest for $K = 1.0$. The velocity field against the similarity variable ξ is shown in Fig. 5. Velocity enhances for higher ξ.

4.2. Temperature

A comparison between trihybrid, hybrid, and nanofluids at $M = 0.1$, $\mathrm{Ec} = 0.5$, $\lambda = 0.01$, $K = 1$ and $\mathrm{Pr} = 6.2$ is illustrated in Fig. 6. The results revealed that the temperature of the hybrid nanofluid and nanofluid declines much faster than that of the trihybrid nanofluid. This means that the fluid temperature was enhanced by adding more nanoparticles to the basefluid. This is due to the fact that the addition of nanomaterials to the basefluid enhances the thermal conductivity of the fluid, causing the

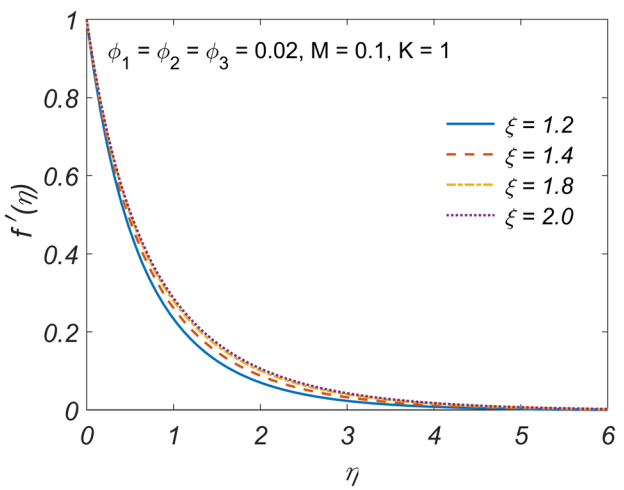

Fig. 5 Similarity variable against velocity.

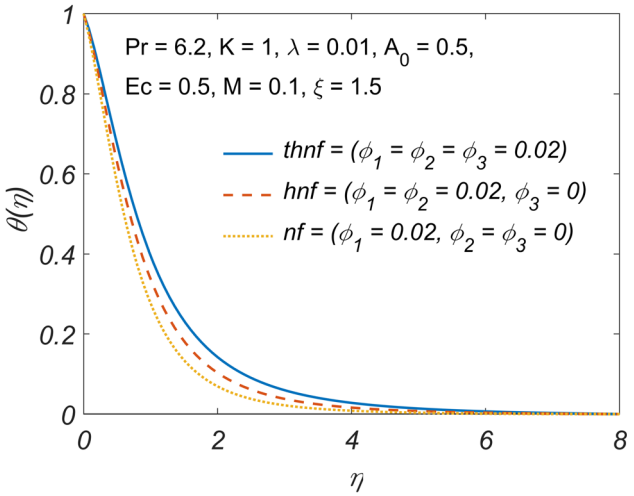

Fig. 6 Comparison of the three different fluids for temperature.

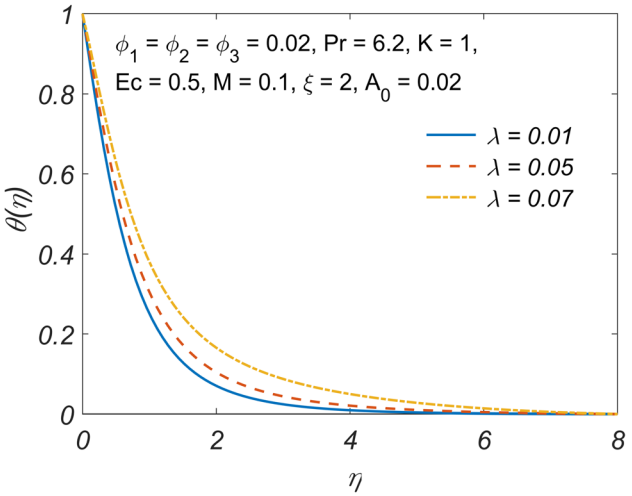

Fig. 9 Heat generation parameter against temperature.

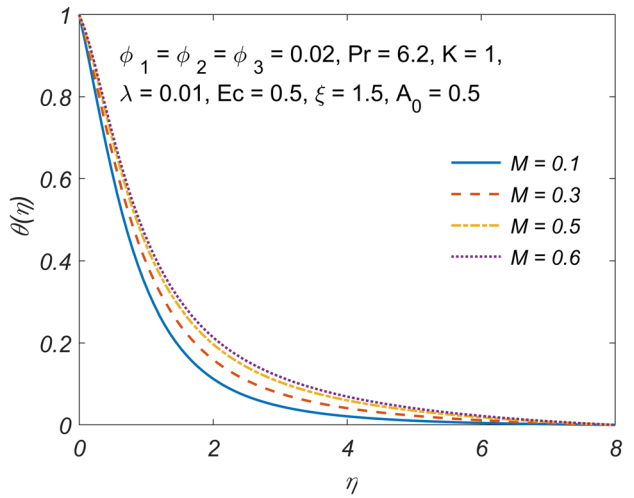

Fig. 7 Magnetic parameter against temperature.

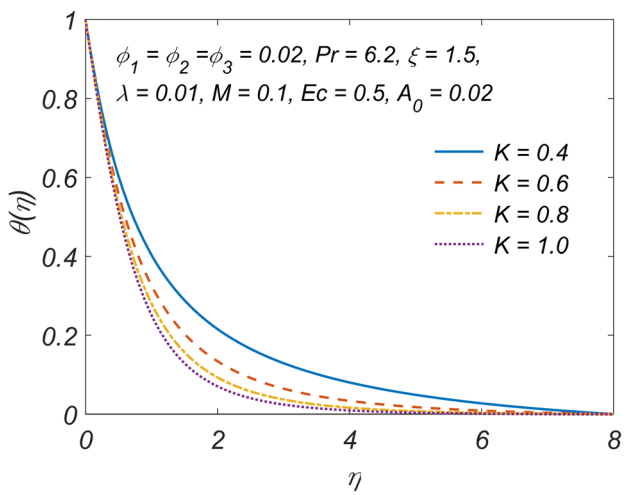

Fig. 10 Curvature parameter against temperature.

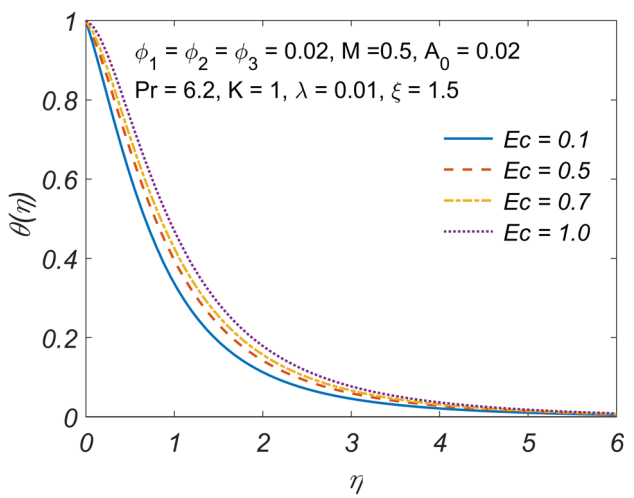

Fig. 8 Eckert number against temperature.

temperature to increase. The relationship between temperature and the magnetic variable is interpreted in Fig. 7. The temperature field grows gradually as the values of the magnetic parameter increase. Physically, when M increases the Lorentz force produces more resistance between fluid particles, which improves the temperature. Fig. 8 illustrates how the Eckert number affects the thermal field. The Eckert number is physically specified as the ratio of kinetic energy to the thermal enthalpy difference. Thus, an increase in temperature for trihybrid nanofluid correlates to the progressive behavior of the Eckert number. Fig. 9 illustrates how a heat generation parameter affects the temperature. Physically, the fluid experiences the improved heat transfer from the surface for higher values of λ. Thus, an increment in λ gives rise to $\theta(\eta)$ as well as thermal layer thickness. Fig. 10 shows the plot of $\theta(\eta)$ against K for the trihybrid nanofluid. In this figure, the temperature and thermal layer thickness decay for higher values of K. Because the curved surface reduces to the flat surfaces when K becomes

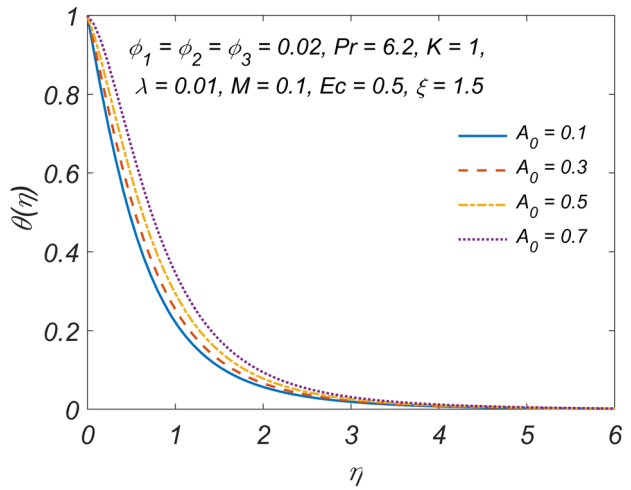

Fig. 11 Temperature exponent against temperature.

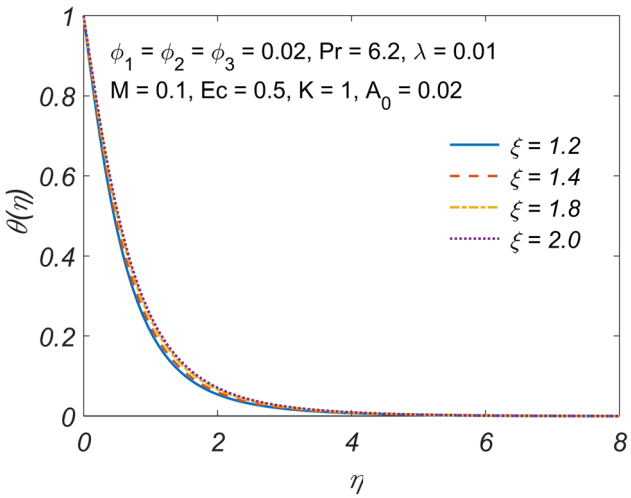

Fig. 12 Similarity variable against temperature.

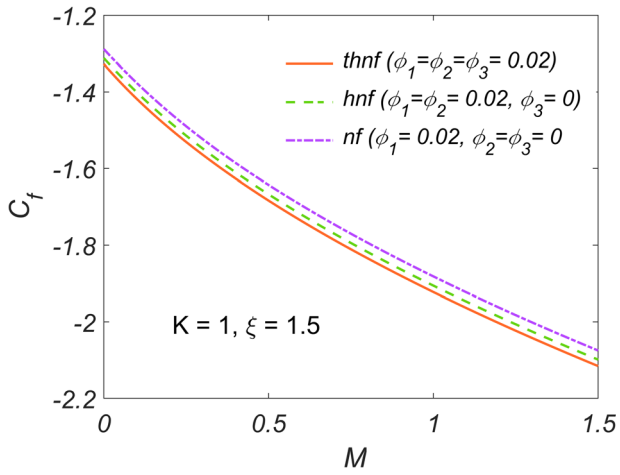

Fig. 13 C_f with M for diverse values of ϕ.

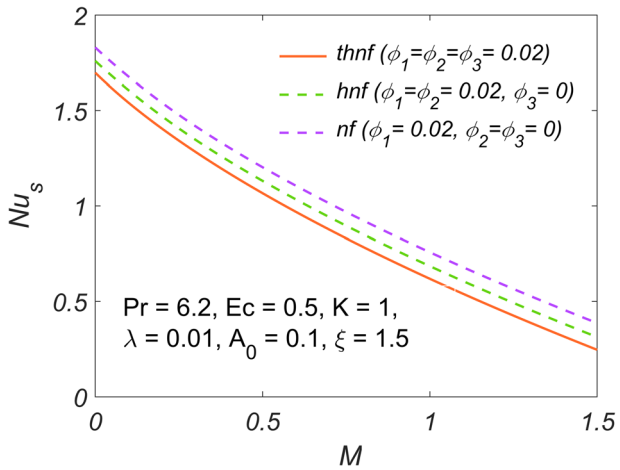

Fig. 14 N_{u_s} with M for diverse values of ϕ.

larger. In this situation, the distance between nanoparticles is growing due to the decline in the curved path, which results in a decrease in the temperature of each nanoparticle. Fig. 11 demonstrates the effect of the temperature exponent on the thermal field. It was observed that the increase in the temperature exponent enhances the thermal field. This leads to thickening in the thermal boundary layer. Similarly, the behavior of the temperature and thermal boundary layer thickness are improved by increasing ξ, as demonstrated in Fig. 12.

4.3. Physical quantities of interest

Characteristics of the interesting parameters such as the magnetic parameter with solid volume fraction (ϕ) on C_f, and N_{u_s} for three different fluids, such as, trihybrid nanofluid, hybrid nanofluid, and nanofluid are explored in this section.

4.3.1. Skin friction coefficient. Fig. 13 shows the surface drag force against the magnetic parameter. It is demonstrated that the magnitude of the skin friction coefficient is enhanced by increasing the values of M. Furthermore, the values of C_f are reduced for the trihybrid nanofluid, as compared to those for the hybrid nanofluid and nanofluid.

Table 4 Comparative study of heat transfer coefficient $-\theta'(0)$ with $K \to \infty$, Ec = 0

Pr	Bidin and Nazar[55]	Khan *et al.*[53]	Present study
1	0.9548	0.954895	0.95485
2	1.4714	1.471635	1.4717
3	1.8691	1.896354	1.8693

4.3.2. Heat transfer rate. Fig. 14 shows the characteristics of M and solid volume fraction on N_{u_s}. Here, N_{u_s} decreases with M. Furthermore, the heat transfer rate is lower for the trihybrid nanofluid as compared to the hybrid nanofluid and nanofluid. The heat transfer rate N_{u_s} is reduced for the larger solid volume fraction ϕ.

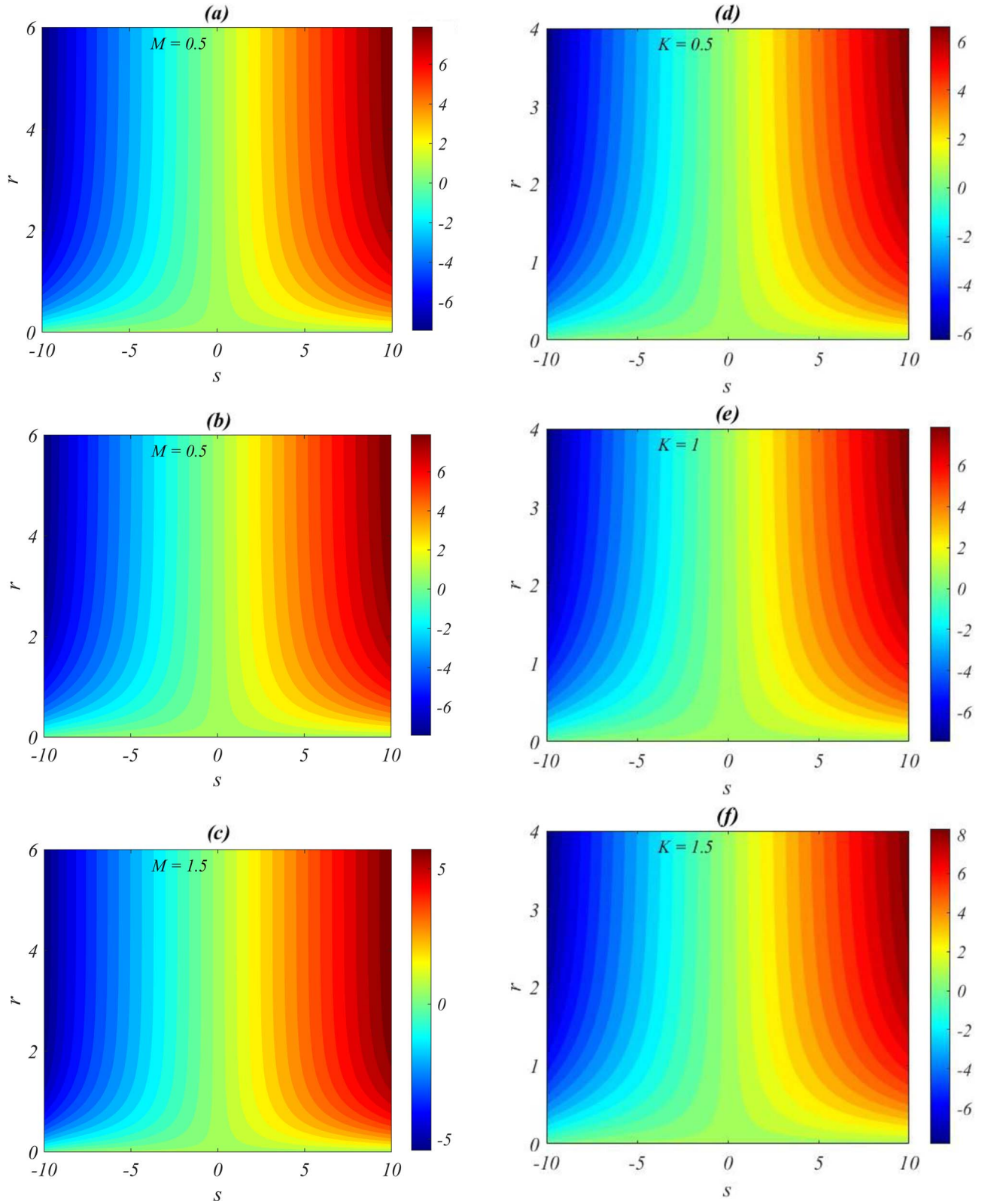

Fig. 15 (a–c) Streamlines for diverse values of M. (d–f) Streamlines for diverse values of K.

4.4. Streamlines

Streamlines are plotted in Fig. 15 to visualize the pattern of the trihybrid (Fe_3O_4, Ag, and Cu) nanofluid flow. Fig. 15(a)–(c) shows how streamlines are drawn for various values of the magnetic parameter M. An increase in the magnetic parameter gives a remarkable shrinking effect for flow sketches. Fig. 15(d)–(f) demonstrates how a useful shrink in the flow

diagrams is produced when the curvature parameter K is increased. Additionally, for higher values of K, there are correspondingly fewer disparities between the flow sketches of the trihybrid nanofluid.

5. Conclusions

In this study, the flow of the MHD trihybrid nanofluid on an exponentially stretchable curved sheet with magnetic field and heat generation effects was investigated. Nanoparticles, such as Fe_3O_4, Ag, and Cu were mixed with water to form a trihybrid nanofluid. The shooting method using the Runge–Kutta–Fehlberg technique was employed to solve the problem. The results were verified by making a comparison with the published work in tabular form. The current problem can be extended to different geometries for many practical applications in the future. This study can be accomplished by using other Newtonian and non-Newtonian fluid models, including the Oldroyd-B fluid model, Casson fluid model, and Walter's B fluid model. Moreover, this problem can be solved by other numerical methods such as the finite difference method and the finite element method. The key outcomes of this study are mentioned below.

- The appearance of trihybrid nanoparticles causes a decrease in the fluid velocity along with the momentum boundary layer thickness, whereas the temperature and thickness of the thermal boundary layer are enhanced.
- The results showed that the trihybrid nanofluid has better thermal conductivity than the basefluid, nanofluid, and hybrid nanofluid.
- The distribution of the temperature increases as the magnetic field grows, whereas the velocity field decreases.
- Higher estimation of K yields an increase in velocity and causes the temperature field to decline.
- A higher temperature field is developed by increasing the heat generation parameter.
- The coefficient of skin friction and local Nusselt number have decreasing effects for ϕ and M.

Nomenclature

Symbols

u, v	Velocity components (m s^{-1})
η, ξ	Similarity variables
r, s	Curvilinear coordinates (m)
M	Magnetic field
R	Radius of sheet (m)
N_{u_s}	Nusselt number
p	Pressure (N m^{-2})
C_f	Skin friction coefficient
T	Fluid temperature (K)
Pr	Prandtl number
T_∞	Ambient temperature (K)
q_w	Heat flux (W m^{-2})
T_0	Reference temperature (K)
τ_{rs}	Shear stress (N m^{-2})
$(\rho C)_f$	Heat capacity (J kg^{-1} K^{-1})
Ec	Eckert number
ν	Kinematic viscosity (m^2 s^{-1})
A_0	Temperature exponent
μ	Dynamic viscosity (kg m^{-1} s^{-1})
k	Thermal conductivity (W m^{-1} K^{-1})
ϕ	Volume fraction (mol L^{-1})
σ	Electrical conductivity (kg^{-1} m^{-3} s^3 A^2)
ρ	Density (kg m^{-3})
λ	Heat generation parameter
U_0	Reference velocity (m s^{-1})
K	Curvature parameter

Subscripts

$i = 1$	For Fe_3O_4 particles
$i = 2$	For Ag particles
$i = 3$	For Cu particles
thnf	Trihybrid nanofluid
hnf	Hybrid nanofluid
nf	Nanofluid
f	Base fluid

Author contributions

W. Shinwari, T. Hayat and Z. Abbas: methodology; writing review and editing. S. Momani: conceptualization; methodology; software; validation; writing original draft preparation; writing review and editing.

Conflicts of interest

There is no conflict of interest among authors to declare.

References

1 A. Acrivos, M. J. Shah and E. E. Petersen, Momentum and heat transfer in laminar boundary-layer flows of non-Newtonian fluids past external surfaces, *AIChE J.*, 1960, **6**(2), 312–317.
2 M. Z. Salleh, R. Nazar and I. Pop, Boundary layer flow and heat transfer over a stretching sheet with Newtonian heating, *J. Taiwan Inst. Chem. Eng.*, 2010, **41**(6), 651–655.
3 H. Xu and S. J. Liao, Laminar flow and heat transfer in the boundary-layer of non-Newtonian fluids over a stretching flat sheet, *Comput. Math. with Appl.*, 2009, **57**(9), 1425–1431.
4 R. Ellahi, S. Z. Alamri, A. Basit and A. Majeed, Effects of MHD and slip on heat transfer boundary layer flow over a moving plate based on specific entropy generation, *J. Taibah Univ. Sci.*, 2018, **12**(4), 476–482.
5 S. K. Khan and E. Sanjayanand, Viscoelastic boundary layer flow and heat transfer over an exponential stretching sheet, *Int. J. Heat Mass Transfer*, 2005, **48**(8), 1534–1542.
6 A. Ishak, R. Nazar and I. Pop, Boundary layer flow and heat transfer over an unsteady stretching vertical surface, *Meccanica*, 2009, **44**(4), 369–375.

7 K. Bhattacharyya, Boundary layer flow and heat transfer over an exponentially shrinking sheet, *Chin. Phys. Lett.*, 2011, **28**(7), 074701.
8 Z. Ahmed, S. Nadeem, S. Saleem and R. Ellahi, Numerical study of unsteady flow and heat transfer CNT-based MHD nanofluid with variable viscosity over a permeable shrinking surface, *Int. J. Numer. Methods Heat Fluid Flow*, 2019, **29**(12), 4607–4623.
9 S. Hoseinzadeh, P. S. Heyns and H. Kariman, Numerical investigation of heat transfer of laminar and turbulent pulsating Al2O3/water nanofluid flow, *Int. J. Numer. Methods Heat Fluid Flow*, 2019, **30**(3), 1149–1166.
10 R. Ellahi, E. Shivanian, S. Abbasbandy and T. Hayat, Numerical study of magnetohydrodynamics generalized Couette flow of Eyring–Powell fluid with heat transfer and slip condition, *Int. J. Numer. Methods Heat Fluid Flow*, 2016, **26**(5), 1433–1445.
11 M. Sajid, N. Ali, T. Javed and Z. Abbas, Stretching a curved surface in a viscous fluid, *Chin. Phys. Lett.*, 2010, **27**, 024703.
12 M. Naveed, M. Imran and Z. Abbas, Curvilinear flow of micropolar fluid with Cattaneo–Christov heat flux model due to oscillation of curved stretchable sheet, *Z. Naturforsch.*, 2021, **76**(9), 799–821.
13 K. Ahmed, W. A. Khan, T. Akbar, G. Rasool, S. O. Alharbi and I. Khan, Numerical investigation of mixed convective Williamson fluid flow over an exponentially stretching permeable curved surface, *Fluids*, 2021, **6**(7), 260.
14 Z. Abbas, M. Naveed and M. Sajid, Hydromagnetic slip flow of nanofluid over a curved stretching surface with heat generation and thermal radiation, *J. Mol. Liq.*, 2016, **215**, 756–762.
15 R. J. Punith Gowda, H. M. Baskonus, R. Naveen Kumar, B. C. Prasannakumara and D. G. Prakasha, Computational investigation of Stefan blowing effect on flow of second-grade fluid over a curved stretching sheet, *Int. J. Appl. Comput. Math.*, 2021, **7**(3), 1–16.
16 M. R. Khan, K. Pan, A. U. Khan and N. Ullah, Comparative study on heat transfer in CNTs-water nanofluid over a curved surface, *Int. Commun. Heat Mass Transfer*, 2020, **116**, 104707.
17 N. S. Wahid, N. M. Arifin, N. S. Khashi'ie, I. Pop, N. Bachok and M. E. H. Hafidzuddin, Flow and heat transfer of hybrid nanofluid induced by an exponentially stretching/shrinking curved surface, *Case Stud. Therm. Eng.*, 2021, **25**, 100982.
18 A. Ali, R. N. Jana and S. Das, Radiative CNT-based hybrid magneto-nanoliquid flow over an extending curved surface with slippage and convective heating, *Heat Transfer*, 2021, **50**(3), 2997–3020.
19 C. M. Mohana and B. Rushi Kumar, Nanoparticle shape effects on MHD Cu–water nanofluid flow over a stretching sheet with thermal radiation and heat source/sink, *Int. J. Mod. Phys. B*, 2023, 2450151.
20 B. Kumar and T. Kumar, A comparative study of thermal radiation effects on MHD flow of nanofluids and heat transfer over a stretching sheet, *Front. Heat Mass Transfer*, 2017, **9**(1), 13.
21 H. Ullah, T. Hayat, S. Ahmad, M. S. Alhodaly and S. Momani, Numerical simulation of MHD hybrid nanofluid flow by a stretchable surface, *Chin. J. Phys.*, 2021, **71**, 597–609.
22 N. Ahmed, F. Saba, U. Khan, S. T. Mohyud-Din, E. S. M. Sherif and I. Khan, Nonlinear thermal radiation and chemical reaction effects on a (Cu–CuO)/NaAlg hybrid nanofluid flow past a stretching curved surface, *Processes*, 2019, **7**(12), 962.
23 D. Lu, M. Ramzan, S. Ahmad, A. Shafee and M. Suleman, Impact of nonlinear thermal radiation and entropy optimization coatings with hybrid nanoliquid flow past a curved stretched surface, *Coatings*, 2018, **8**(12), 430.
24 Y. M. Chu, S. Bashir, M. Ramzan and M. Y. Malik, Model-based comparative study of magnetohydrodynamics unsteady hybrid nanofluid flow between two infinite parallel plates with particle shape effects, *Math. Methods Appl. Sci.*, 2023, **46**(10), 11568–11582.
25 M. A. Sadiq, F. Haider and T. Hayat, Entropy generation analysis of hybrid nanomaterial through porous space with variable characteristics, *Entropy*, 2021, **23**(1), 89.
26 S. Jana, A. Salehi-Khojin and W. H. Zhong, Enhancement of fluid thermal conductivity by the addition of single and hybrid nano-additives, *Thermochim. Acta*, 2007, **462**(1–2), 45–55.
27 S. S. U. Devi and S. A. Devi, Numerical investigation of three-dimensional hybrid Cu–Al2O3/water nanofluid flow over a stretching sheet with effecting Lorentz force subject to Newtonian heating, *Can. J. Phys.*, 2016, **94**(5), 490–496.
28 S. Nadeem, N. Abbas and M. Y. Malik, Inspection of hybrid based nanofluid flow over a curved surface, *Comput. Methods Programs Biomed.*, 2020, **189**, 105193.
29 H. A. Nabwey and A. Mahdy, Transient flow of micropolar dusty hybrid nanofluid loaded with Fe3O4-Ag nanoparticles through a porous stretching sheet, *Results Phys.*, 2021, **21**, 103777.
30 T. Hayat and S. Nadeem, Heat transfer enhancement with Ag–CuO/water hybrid nanofluid, *Results Phys.*, 2017, **7**, 2317–2324.
31 F. Ahmad, S. Abdal, H. Ayed, S. Hussain, S. Salim and A. O. Almatroud, The improved thermal efficiency of Maxwell hybrid nanofluid comprising of graphene oxide plus silver/kerosene oil over stretching sheet, *Case Stud. Therm. Eng.*, 2021, **27**, 101257.
32 M. Haneef, H. A. Madkhali, A. Salmi, S. O. Alharbi and M. Y. Malik, Numerical study on heat and mass transfer in Maxwell fluid with tri and hybrid nanoparticles, *Int. Commun. Heat Mass Transfer*, 2022, **135**, 106061.
33 S. Manjunatha, V. Puneeth, B. J. Gireesha and A. Chamkha, Theoretical study of convective heat transfer in ternary nanofluid flowing past a stretching sheet, *J. Appl. Comput. Mech.*, 2022, **8**(4), 1279–1286.
34 A. I. Ramadhan, W. H. Azmi, R. Mamat, K. A. Hamid and S. Norsakinah, Investigation on stability of tri-hybrid nanofluids in water-ethylene glycol mixture, *Mater. Sci. Eng.*, 2019, **469**, 012068.
35 J. Hasnain and N. Abid, Numerical investigation for thermal growth in water and engine oil-based ternary nanofluid

using three different shaped nanoparticles over a linear and nonlinear stretching sheet, *Numer. Heat Transfer*, 2023, **83**(12), 1365–1376.

36 M. Sohail, E. R. El-Zahar, A. Mousa, U. Nazir, S. Althobaiti, A. Althobaiti, N. A. Shah and J. D. Chung, Finite element analysis for ternary hybrid nanoparticles on thermal enhancement in pseudo-plastic liquid through porous stretching sheet, *Sci. Rep.*, 2022, **12**(1), 9219.

37 F. Fangfang, T. Sajid, W. Jamshed, M. R. Eid, G. C. Altamirano, I. Altaf and S. M. El Din, Thermal transport and characterized flow of trihybridity Tiwari and Das Sisko nanofluid via a stenosis artery, A case study, *Case Stud. Therm. Eng.*, 2023, **47**, 103064.

38 T. Sajid, A. A. Pasha, W. Jamshed, F. Shahzad, M. R. Eid, R. W. Ibrahim and S. M. El Din, Radiative and porosity effects of trihybrid Casson nanofluids with Bödewadt flow and inconstant heat source by Yamada-Ota and Xue models, *Alexandria Eng. J.*, 2023, **66**, 457–473.

39 N. A. S. Muzaidi, M. A. Fikri, K. N. S. W. S. Wong, A. Z. M. Sofi, R. Mamat, N. M. Adenam, M. Y. Yunin and H. K. Adli, Heat absorption properties of CuO/TiO2/SiO2 trihybrid nanofluids and its potential future direction towards solar thermal applications, *Arabian J. Chem.*, 2021, **14**(4), 103059.

40 F. Shahzad, W. Jamshed, M. R. Eid, R. W. Ibrahim, F. Aslam, S. S. P. M. Isa and K. Guedri, The effect of pressure gradient on MHD flow of a tri-hybrid Newtonian nanofluid in a circular channel, *J. Magn. Magn. Mater.*, 2023, **568**, 170320.

41 A. Rauf, N. A. Shah and T. Botmart, Hall current and morphological effects on MHD micropolar non-Newtonian tri-hybrid nanofluid flow between two parallel surfaces, *Sci. Rep.*, 2022, **12**(1), 16608.

42 Z. Xuan, Y. Zhai, M. Ma, Y. Li and H. Wang, Thermo-economic performance and sensitivity analysis of ternary hybrid nanofluids, *J. Mol. Liq.*, 2021, **323**, 114889.

43 E. M. Sparrow, H. Quack and C. J. Boerner, Local non-similarity boundary layer solutions, *AIAA J.*, 1970, **8**, 1936–1942.

44 A. Raees, U. Farooq, M. Hussain, W. A. Khan and F. B. Farooq, Non-similar mixed convection analysis for magnetic flow of second-grade nanofluid over a vertically stretching sheet, *Commun. Theor. Phys.*, 2021, **73**(6), 065801.

45 P. M. Patil, D. N. Latha, S. Roy and E. Momoniat, Non-similar solutions of mixed convection flow from an exponentially stretching surface, *Ain Shams Eng. J.*, 2017, **8**(4), 697–705.

46 U. Farooq, M. A. Ijaz, M. I. Khan, S. S. P. M. Isa and D. C. Lu, Modeling and non-similar analysis for Darcy–Forchheimer–Brinkman model of Casson fluid in a porous media, *Int. Commun. Heat Mass Transfer*, 2020, **119**, 104955.

47 A. K. Ray, B. Vasu, P. V. S. N. Murthy and R. S. Gorla, Non-similar solution of Eyring–Powell fluid flow and heat transfer with convective boundary condition: homotopy Analysis Method, *Int. J. Appl. Comput. Math.*, 2020, **6**, 16.

48 T. Hayat, S. A. Khan, A. Alsaedi and Q. Z. Zai, Computational analysis of heat transfer in mixed convective flow of CNTs with entropy optimization by a curved stretching sheet, *Int. Commun. Heat Mass Transfer*, 2020, **118**, 104881.

49 E. A. Algehyne, E. R. El-Zahar, M. Sohail, U. Nazir, H. A. AL-bonsrulah, D. Veeman and F. M. Alharbi, Thermal improvement in pseudo-plastic material using ternary hybrid nanoparticles via non-Fourier's law over porous heated surface, *Energies*, 2021, **14**(23), 8115.

50 J. Raza, A. M. Rohni and Z. Omar, Numerical investigation of copper–water (Cu–water) nanofluid with different shapes of nanoparticles in a channel with stretching wall: slip effects, *Math. Comput. Appl.*, 2016, **21**(4), 43.

51 M. Rashid, T. Hayat, A. Alsaedi and B. Ahmed, Flow of Fe3O4 nanofluid with dust and nanoparticles, *Appl. Nanosci.*, 2020, **10**(8), 3115–3122.

52 N. Abid, M. Ramzan, J. D. Chung, S. Kadry and Y. M. Chu, Comparative analysis of magnetized partially ionized copper, copper oxide–water and kerosene oil nanofluid flow with Cattaneo–Christov heat flux, *Sci. Rep.*, 2020, **10**(1), 1–14.

53 S. A. Khan, T. Hayat and A. Alsaedi, Thermal radiation impact on chemical reactive flow of micropolar nanomaterial subject to Brownian diffusion and thermophoresis phenomenon, *J. Comput. Theor. Sci.*, 2023, 102094.

54 T. Hayat, A. Kiran, M. Imtiaz and A. Alsaedi, Hydromagnetic mixed convection flow of copper and silver water nanofluids due to a curved stretching sheet, *Results Phys.*, 2016, **6**, 904–910.

55 B. Bidin and R. Nazar, Numerical solution of the boundary layer flow over an exponentially stretching sheet with thermal radiation, *Eurasian J. Sci. Res.*, 2009, **33**, 710–717.